POLISH MARITIME RESEARCH 1 (121) 2024 Vol. 31; pp. 114-126
10.2478/pomr-2024-0012

PRACTICAL FINITE-TIME EVENT-TRIGGERED CONTROL OF UNDERACTUATED SURFACE VESSELS IN PRESENCE OF FALSE DATA INJECTION ATTACKS

Liping Chen*
School of Ocean Information Engineering, Jimei University, Xiamen, China
Minghua Sun
College of Navigation, Jimei University, Xiamen 361021, Fujian, China
Li Wang
Department of Youth League Committee, Jinan Vocational College of Engineering, Jinan, China

* Corresponding author: *lpchen@jmu.edu.cn (Liping Chen)*

ABSTRACT

The results of studies on a trajectory-tracking problem affected by false data injection attacks (FDIAs) and internal and external uncertainties are presented in this paper. In view of the FDIAs experienced by the system, we compensate for the serious navigation deviation caused by malicious attacks by designing an online approximator. Next, we study the internal and external uncertainties introduced by environmental factors, system parameter fluctuations, or sensor errors, and we design adaptive laws for these uncertainties to approximate their upper bounds. To further enhance the response velocity and stability of the system, we introduce finite-time technology to ensure that the unmanned underactuated surface vessels (USVs) reach the predetermined trajectory-tracking target within finite time. To further reduce the update frequency of the controller, we introduced event-triggered control (ETC) technology. This saves the system's communication resources and optimizes the system. Through Lyapunov stability theory, a strict and complete stability analysis is provided for the control scheme. Finally, the effectiveness of the control scheme is verified using two sets of simulations.

Keywords: Unmanned underactuated surface vessels; False data injection attacks; Internal and external uncertainty; Finite-time control; Event-triggered control

INTRODUCTION

In recent years, unmanned underactuated surface vessels (USVs) have received widespread attention due to the continuous development of the maritime economy [1]. Unmanned USVs lack lateral drive, which requires researchers to consider more aspects when they design control schemes [2]. We are currently in the information age, and unmanned USVs are also susceptible to cyber-attacks. In particular, false data injection attacks (FDIAs) can cause serious navigation deviations in USVs [3]. Therefore, a more complete control scheme must be designed to deal with the above challenges.

In practice, USVs are inevitably affected by external interference. Under the constraints of external interference, feedback linearization is the most commonly used design method [4]. This method makes the problem simple by introducing appropriate feedback to linearize some parts of or the entire nonlinear system. However, although nonlinear problems can be transformed into linear problems through this method, complex mathematical transformations may be required to achieve this transformation. To avoid similar problems, the authors of [5] automatically adjusted the parameters to respond to environmental changes by introducing adaptive technology. This approach caused the control design to no longer be dependent on an accurate

system model. However, adaptive controllers may overreact to noise or brief perturbations, resulting in unnecessary controller adjustments. To further optimize control, the authors of [6], [7] introduced a disturbance observer (DO) to estimate and compensate for external disturbances in real time. Although the perturbation observer does not completely rely on an accurate system model, it requires some prior knowledge of the model. Therefore, usually, the DO will combine adaptive neural networks (NNs), fuzzy control, and other methods to design the control scheme. The authors of [1] further introduced a finite-time disturbance observer (FTDO) to compensate for external interference. The FTDO can complete disturbance estimation within finite time, which makes its response to disturbances faster than that of the traditional DO.

Due to the modelling technology and the complex structure of the USV itself, the USV mathematical model has unmodelled dynamics. These uncertain dynamics caused by model parameter perturbations, unmodelled dynamics, etc., are called internal uncertainties. The authors of [8] designed a control scheme by combining model predictive control (MPC) and online parameter estimation technology. When system parameters change or there is a disturbance, this scheme uses online estimated parameters to update the model, thereby adapting to the uncertain dynamics of the system to a certain extent [9]. However, MPC needs to solve an optimization problem at each control step. For a system with multiple constraints, the computational complexity will increase dramatically. In addition, the performance of MPC is highly dependent on the accuracy of the model used. If the model deviates significantly from the real system, it may not achieve the desired performance [10]. The authors of [11], [12] used fuzzy and neural networks, respectively, to reconstruct the uncertain dynamics of the system. However, they also face the same problem as MPC, that is, the computing requirements of the system can be high. The authors of [13], [14] used the output feedback design method to estimate the unmeasured state within the system. Compared with NNs, state observers provide a structured approach for estimating unmeasured states. The design logic and principles are usually clear and explainable. The NNs are often regarded as 'black box' models, and their inner workings are difficult to explain. However, the performance of state observers is often highly dependent on accurate knowledge of the system model. If the system model is inaccurate or contains significant modelling errors, the performance of the observer may be severely affected.

In practice, to ensure the safety of the USVs, trajectory tracking needs to be completed within finite time. This may be difficult to achieve with traditional control strategies. Unlike traditional asymptotic stability control strategies, finite time control (FTC) strategies ensure stability and a given tracking performance within a predetermined time. The authors of [15]–[17] designed a finite-time trajectory-tracking control scheme. They reduced possible instability or undesirable behaviour during the transition by reducing the transition time of the system from the initial state to the desired state. The authors of [1], [18] further introduced FTDO based on [15]–[17], which further improved the steady-state performance of the system. The control signal updates of most of the above control schemes are based on predetermined, fixed time intervals, without considering the system status or external events. Event-triggered control (ETC) only updates control inputs when certain events or conditions are met, rather than at fixed time intervals. Compared with fixed time intervals, communication bandwidth can be saved and energy consumption can be reduced [19], [20]. The authors of [19] designed a model-based time-triggered control scheme. The authors of [20] further considered actuator faults and designed an adaptive Proportional-integral-derivative (PID) fault-tolerant control scheme based on ETC. However, none of the above literature considers the potential impact of the network environment on the USV system.

The authors of [21] developed a predictive compensator based on event-triggered model predictive control. This strategy can mitigate the effects of external interference and input restrictions under cyberattacks such as denial of service (DoS) attacks. The integration of a model predictive controller with a nonlinear disturbance observer in this strategy enables the precise estimation of and compensation for disturbances. In addition, the predictive compensator effectively reduces the impact of cyberattacks, while the event-triggering mechanism saves computing resources. The authors of [22] discussed the security control of multiple autonomous ground vehicles when they faced DoS network attacks and proposed a distributed security formation control algorithm. The algorithm optimizes communication resources using a model-based dynamic event-triggering mechanism and a positive minimum inter-event time. The authors of [23] studied the adaptive event-triggered path tracking control of a USV based on double-layer virtual ship guidance under spoofing attacks. They introduced an adaptive virtual ship model for smooth path generation and a robust adaptive control algorithm to compensate for spoofing attacks. This method combines event-triggering rules with adaptive compensation technology to improve the accuracy and stability of the closed-loop control system. These studies provide innovative solutions for USV security against cybersecurity threats. The above literature did not consider FDIAs.

In the current network security environment, USVs face the threat of multiple network attacks. FDIAs represent a particularly serious threat. This attack disrupts the normal operation of the ship by injecting false or misleading information into the system.

PROBLEM FORMULATION AND PRELIMINARIES

In this paper, we use a mathematical model of USVs with three degrees of freedom. The model contains information such as the USV's mass, displacement, and yaw moment. The specific form is as follows [24] [25]:

$$\begin{cases} \dot{x} = u\cos(\varphi) - v\sin(\varphi) \\ \dot{y} = u\sin(\varphi) + v\cos(\varphi) \\ \dot{\varphi} = r \end{cases} \tag{1}$$

$$\begin{cases} \dot{u} = \dfrac{1}{m_u}\left[\tau_u{}^f + f_u(V) + d_u\right] \\ \dot{v} = \dfrac{1}{m_v}\left[f_v(V) + d_v\right] \\ \dot{r} = \dfrac{1}{m_r}\left[\tau_r{}^f + f_r(V) + d_r\right] \end{cases} \tag{2}$$

$$\begin{cases} f_u(V) = (m_v vr - Y_r r^2 + X_u u + X_{u|u|}|u|u) \\ f_v(V) = (Y_v v + Y_{|v|v}|v|v + Y_{|r|v}|r|v + Y_r r - m_u ur + Y_{|v|r}|v|r + Y_{|r|r}|r|r) \\ f_r(V) = [(m_u - m_v)uv + Y_r ur + N_v v + N_r r + N_{|r|v}|r|v + N_{|v|v}|v|v + N_{|v|r}|v|r + N_{|r|r}|r|r] \end{cases} \tag{3}$$

where x, y, and φ represent the position and heading angle of the USV in the geodetic coordinate system, respectively. u, v, and r represent the velocity of the USV in different directions, respectively. $f_u(V)$, $f_v(V)$, and $f_r(V)$ represent nonlinear dynamics. $m_i\,(i = u,v,r)$ represents inertial masses. d_u, d_v, and d_r represent external interference items. $\tau_u{}^f$ and $\tau_r{}^f$ are the control inputs disturbed by the FDIAs. The mathematical expressions for these variables are as follows [26]:

$$\begin{cases} \tau_u{}^f = \tau_u + \xi_u \\ \tau_r{}^f = \tau_r + \xi_r \end{cases} \tag{4}$$

where ξ_u and ξ_r are the FDIAs experienced by the system.

Remark 1: The physical equipment and controllers of autonomous unmanned vessels are often connected to each other through networks. This connection method makes the system vulnerable to cyberattacks. The focus of this article is to explore a specific form of attack related to Eq. (3), namely additive FDIAs. The core principle of this attack is that the attacker maliciously injects false signals into the communication link between the controller and the actuator, thereby affecting or destroying the normal operation of the system. Such attacks can have serious negative impacts on the safety and performance of autonomous unmanned vessels.

The assumptions and required lemmas in this study are as follows:

Assumption 1 [25]**:** The $f_i(V)$, $i = (u,v,r)$, are unknown. Interference items outside the system, that is, external interference d_i, $i = (u,v,r)$, are unknown and bounded. That is, there are unknown positive constants η_i, such that d_i satisfies $|d_i| \le \eta_i$.

Assumption 2: The sway velocity is passively bounded.

Lemma 1 [27]**:** Assume that there is a positive definite Lyapunov function $V(x): \Omega_0 \to R$ and any scalars $a > 0$, $b > 0$, and $0 < \kappa < 1$, so that the inequality $\dot{V}(x) + aV(x) + bV^{\kappa}(x) \le 0$ holds; then, the system is stable in finite time, and its adjustment time satisfies

$$T \le \frac{1}{a(1-t)} \ln \frac{aV^{1-\kappa}(x_0) + b}{b} \tag{4}$$

where $V(x_0)$ is the initial value of $V(x)$.

Lemma 2 [28] [29]**:** For any $\lambda > 0$ and $x \in R$, the following relationship is satisfied:

$$0 < |x| - x\tanh\left(\frac{x}{\lambda}\right) \le 0.2785\lambda \tag{5}$$

CONTROL DESIGN AND STABILITY ANALYSIS

DESIGN OF VIRTUAL CONTROL LAWS

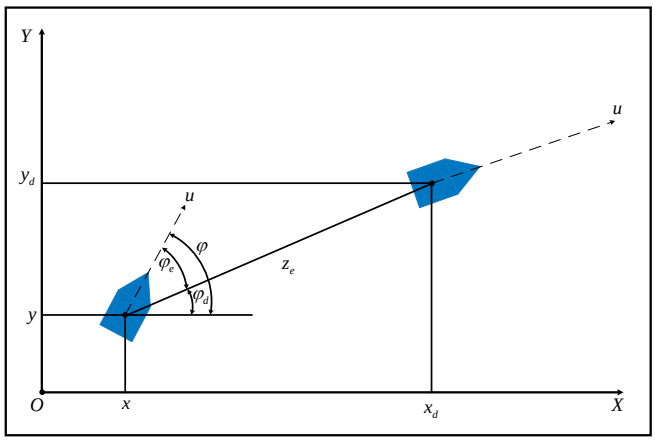

Fig. 1. General framework of USV trajectory-tracking control

The tracking error is defined as follows:

$$\begin{bmatrix} x_e \\ y_e \\ \varphi_e \end{bmatrix} = J^{\mathrm{T}}(\varphi) \begin{bmatrix} x - x_d \\ y - y_d \\ \varphi - \varphi_d \end{bmatrix} \tag{6}$$

$$J^{\mathrm{T}}(\varphi) = \begin{bmatrix} \cos\varphi & \sin\varphi & 0 \\ -\sin\varphi & \cos\varphi & 0 \\ 0 & 0 & 1 \end{bmatrix} \tag{7}$$

where x_e is the lateral error, y_e is the longitudinal error, φ_e is the heading angle error, and $z_e = \sqrt{x_e^2 + y_e^2}$ [23]. $J^{-1}(\varphi)$ is a rotation matrix, and $J^{\mathrm{T}}(\varphi) \quad J^{-1}(\varphi)$. x_d, y_d, and φ_d are the reference position and reference heading angle, respectively. α_u and α_r are virtual control variables designed later. The specific form of the reference heading is as follows:

$$\varphi_d = \begin{cases} \arctan\left(\dfrac{\dot{y}_d}{\dot{x}_d}\right), & z_e = 0 \\ 0.5\left[1 - \operatorname{sgn}(x_e)\right]\operatorname{sgn}(y_e) + \arctan\left(\dfrac{y_e}{x_e}\right), & \text{other} \end{cases} \tag{8}$$

Then, we can obtain the new kinematic error equation as follows:

$$\begin{cases} x_e = z_e \cos\varphi_d \\ y_e = z_e \sin\varphi_d \\ \varphi_e = \varphi - \varphi_d \end{cases} \tag{9}$$

The Lyapunov function is defined as follows:

$$H_1 = \frac{1}{2} z_e^{\,2} + \frac{1}{2}\varphi_e^{\,2} \tag{10}$$

By deriving Eq. (10), we can obtain

$$\begin{aligned} \dot{H}_1 &= z_e \dot{z}_e + \varphi_e \dot{\varphi}_e = x_e \dot{x}_e + y_e \dot{y}_e + \varphi_e \dot{\varphi}_e \\ &= z_e\left[\cos\varphi_d\left(\dot{x} - \dot{x}_d\right) + \sin\varphi_d\left(\dot{y} - \dot{y}_d\right)\right] + \varphi_e\left(r - \dot{\varphi}_d\right) \\ &= z_e\left[u_e\cos\varphi_e - v\sin\varphi_e + \alpha_u\cos\varphi_e - \dot{x}_d\cos\varphi_d - \dot{y}_d\sin\varphi_d\right] + \varphi_e\left(r - \dot{\varphi}_d\right) \end{aligned} \tag{11}$$

According to Eq. (11), the virtual control variables are designed as follows:

$$\begin{cases} \alpha_u = \dfrac{1}{\cos\varphi_e}\left[\eta_{11} z_e + \eta_{12} sig^{\nu}(z_e) + \dot{x}_d\cos\varphi_d + \dot{y}_d\sin\varphi_d + v\sin\varphi_e\right] \\ \alpha_r = -\eta_{21}\varphi_e - \eta_{22} sig^{\nu}(\varphi_e) + \dot{\varphi}_d \end{cases} \tag{12}$$

where η_{11}, η_{12}, η_{21}, η_{22}, and ν are positive definite parameters. $sig^{\upsilon}(.) = |.|^{\nu}\operatorname{sgn}(.)$。, where $\operatorname{sgn}(.)$ is the sign function.

SURGE AND YAW ADAPTIVE CONTROL LAWS DESIGN

To avoid the derivation of the virtual controls α_u and α_r, we introduce the following filter:

$$\begin{cases} \kappa_u \dot{\beta}_u + \beta_u = \alpha_u \\ \kappa_r \dot{\beta}_r + \beta_r = \alpha_r \end{cases} \tag{13}$$

where κ_u and κ_r are positive definite parameters.

According to Eq. (13), the filter error is defined as follows:

$$\begin{cases} e_u{}^f = \beta_u - \alpha_u \\ e_r{}^f = \beta_r - \alpha_r \end{cases} \tag{14}$$

By deriving Eq. (14), we can obtain

$$\begin{cases} \dot{e}_u{}^f = \dot{\beta}_u - \dot{\alpha}_u \\ \dot{e}_r{}^f = \dot{\beta}_r - \dot{\alpha}_r \end{cases} \tag{15}$$

Substituting Eq. (12) into Eq. (15), we can obtain

$$\begin{cases} \dot{e}_u{}^f = \dot{\beta}_u - \dot{\alpha}_u = -\dfrac{e_u}{\kappa_u} + \chi_u \\ \dot{e}_r{}^f = \dot{\beta}_r - \dot{\alpha}_r = -\dfrac{e_r}{\kappa_r} + \chi_r \end{cases} \tag{16}$$

where χ_u and χ_r are continuous bounded functions, and the maximum values are P_u and P_r.

The velocity tracking error is defined as follows:

$$\begin{cases} u_e = u - \beta_u \\ r_e = r - \beta_r \end{cases} \tag{17}$$

By taking the time derivative of Eq. (17) and substituting Eqs. (2) and (3) into it, we can obtain

$$\begin{cases} m_u \dot{u}_e = \tau_u + \Theta_u + \xi_{d_u} - m_u \dot{\beta}_u \\ m_r \dot{r}_e = \tau_r + \Theta_r + \xi_{d_r} - m_r \dot{\beta}_r \end{cases} \tag{18}$$

where $\xi_{d_u} = \xi_u + \bar{d}_u$, $\xi_{d_r} = \xi_r + \bar{d}_r$, $\Theta_u = \bar{f}_u(V)$, and $\Theta_r = \bar{f}_r(V)$. $\bar{d}_u$, $\bar{d}_r$, $\bar{f}_u(V)$, and $\bar{f}_r(V)$ are the upper bounds of d_u, d_r, $f_u(V)$, and $f_r(V)$, respectively.

The design control law and adaptive law are as follows:

$$\begin{cases} \tau_u = -\eta_{31}u_e - \eta_{32}sig^{\upsilon}(u_e) - \hat{\Theta}_u - \hat{\xi}_{d_u} - |z_e \cos\varphi_e| + m_u\dot{\beta}_u \\ \dot{\hat{\Theta}}_u = \mu_u\left[\tanh\left(\frac{u_e}{\delta_{\vartheta_u}}\right)u_e - \vartheta_u\Theta_u\right] \\ \dot{\hat{\xi}}_{d_u} = \varepsilon_u\left[\tanh\left(\frac{u_e}{\delta_{\phi_u}}\right)u_e - \phi_u\xi_{d_u}\right] \\ \tau_r = -\eta_{41}r_e - \eta_{42}sig^{\upsilon}(r_e) - \hat{\Theta}_r - \hat{\xi}_{d_r} - \varphi_e + m_r\dot{\beta}_r \\ \dot{\hat{\Theta}}_r = \mu_r\left[\tanh\left(\frac{r_e}{\delta_{\vartheta_r}}\right)r_e - \vartheta_r\hat{\Theta}_r\right] \\ \dot{\hat{\xi}}_{d_r} = \varepsilon_r\left[\tanh\left(\frac{r_e}{\delta_{\phi_r}}\right)r_e - \phi_r\xi_{d_r}\right] \end{cases} \quad (19)$$

where η_{31}, η_{32}, μ_u, ϑ_u, δ_{ϑ_u}, ε_u, ϕ_u, δ_{ϕ_u}, η_{41}, η_{42}, μ_r, ϑ_r, δ_{ϑ_r}, ε_r, ϕ_r, and δ_{ϕ_r} are positive definite parameters. $\hat{\Theta}_u$, $\hat{\Theta}_r$, $\hat{\xi}_{d_u}$, and $\hat{\xi}_{d_r}$ are the estimated values of Θ_u, Θ_r, ξ_{d_u}, and ξ_{d_r}, respectively.

Define the measurement error as

$$\begin{cases} e_u(t) = L_u(t) - \tau_u(t),\ t \in [t_k, t_{k+1}) \\ e_r(t) = L_r(t) - \tau_r(t),\ t \in [t_k, t_{k+1}) \end{cases} \quad (20)$$

where t is the trigger time interval, $\tau_u(t)$ and $\tau_r(t)$ are the values of the controller at the previous starting time, and $\tau_u(t)$ and $\tau_r(t)$ will start at the trigger time t_k and will be maintained at a constant value by the zero-order holder until the trigger time t_{k+1} is updated.

The design ETC conditions are as follows:

$$\begin{cases} \tau_u(t) = L_u(t_k), \forall t \in [t_k, t_{k+1}) \\ t_{k+1} = \inf\left\{t \in R \middle| |e_u(t)| \geq \eta_u\right\} \end{cases} \quad (21)$$

$$\begin{cases} \tau_r(t) = L_r(t_k), \forall t \in [t_k, t_{k+1}) \\ t_{k+1} = \inf\left\{t \in R \middle| |e_r(t)| \geq \eta_r\right\} \end{cases} \quad (22)$$

where η_u and η_r are design parameters greater than 0. When the trigger condition is violated, the update time of the controller is marked as t_{k+1}, and the control signal of the controller is simultaneously updated as $\omega_u(t_{k+1})$ as the control input of the system.

STABILITY ANALYSIS

Select the following Lyapunov function for the closed-loop system:

$$H = H_1 + \frac{m_u}{2}u_e^2 + \frac{m_r}{2}r_e^2 + \frac{1}{2}\left(e_u^f\right)^2 + \frac{1}{2}\left(e_r^f\right)^2 + \frac{1}{2\mu_u}\tilde{\Theta}_u^2 + \frac{1}{2\mu_r}\tilde{\Theta}_r^2 + \frac{1}{2\varepsilon_u}\tilde{\xi}_{d_u}^2 + \frac{1}{2\varepsilon_r}\tilde{\xi}_{d_r}^2 \quad (23)$$

where $\tilde{\Theta}_u$, $\tilde{\Theta}_r$, $\tilde{\xi}_{d_u}$, and $\tilde{\xi}_{d_r}$ are the estimation errors of Θ_u, Θ_r, ξ_{d_u}, and ξ_{d_r}, respectively.

By deriving Eq. (23) and substituting Eq.(19) into it, we can obtain

$$\begin{aligned} \dot{H} = {} & \dot{H}_1 + m_u u_e\dot{u}_e + m_r r_e\dot{r}_e + e_u^f\dot{e}_u^f + e_r^f\dot{e}_r^f - \frac{1}{\mu_u}\tilde{\Theta}_u\dot{\hat{\Theta}}_u - \frac{1}{\mu_r}\tilde{\Theta}_r\dot{\Theta}_r - \frac{1}{\varepsilon_u}\tilde{\xi}_{d_u}\dot{\hat{\xi}}_{d_u} - \frac{1}{\varepsilon_r}\tilde{\xi}_{d_r}\dot{\xi}_{d_r} \\ & - \eta_{11}z_e^2 - \eta_{12}|z_e|^{\upsilon+1}\mathrm{sgn}(z_e) + z_e u_e\cos\varphi_e - \eta_{21}\varphi_e^2 - \eta_{22}|\varphi_e|^{\upsilon+1}\mathrm{sgn}(\varphi_e) + \varphi_e r_e \\ & + u_e\left[-\eta_{31}u_e - \eta_{32}|u_e|^{\upsilon}\mathrm{sgn}(u_e) - |z_e\cos\varphi_e| + \tilde{\Theta}_u + \tilde{\xi}_{d_u}\right] + r_e\left[-\eta_{41}r_e - \eta_{42}|r_e|^{\upsilon}\mathrm{sgn}(r_e) - \varphi_e + \tilde{\Theta}_r + \tilde{\xi}_{d_r}\right] \\ & - \tilde{\Theta}_u\left[\tanh\left(\frac{u_e}{\delta_{\vartheta_u}}\right)u_e - \vartheta_u\hat{\Theta}_u\right] - \tilde{\Theta}_r\left[\tanh\left(\frac{r_e}{\delta_{\vartheta_r}}\right)r_e - \vartheta_r\Theta_r\right] \\ & - \tilde{\xi}_{d_u}\left[\tanh\left(\frac{u_e}{\delta_{\phi_u}}\right)u_e - \phi_u\hat{\xi}_{d_u}\right] - \tilde{\xi}_{d_r}\left[\tanh\left(\frac{r_e}{\delta_{\phi_r}}\right)r_e - \phi_r\xi_{d_r}\right] \\ & - \frac{\left(e_u^f\right)^2}{\kappa_u} + e_u^f P_u - \frac{\left(e_r^f\right)^2}{\kappa_r} + e_r^f P_r \end{aligned} \quad (24)$$

According to Lemma 2, Eq. (24) can become

$$\begin{aligned} \dot{H} \leq {} & -\eta_{11}z_e^2 - \eta_{12}|z_e|^{\upsilon+1}\mathrm{sgn}(z_e) - \eta_{21}\varphi_e^2 - \eta_{22}|\varphi_e|^{\upsilon+1}\mathrm{sgn}(\varphi_e) \\ & - \eta_{31}u_e^2 - \eta_{32}|u_e|^{\upsilon+1}\mathrm{sgn}(u_e) - \eta_{41}r_e^2 - \eta_{42}|r_e|^{\upsilon+1}\mathrm{sgn}(r_e) \\ & + 0.2785\delta_{\vartheta_u}\tilde{\Theta}_u + \vartheta_u\tilde{\Theta}_u\left(\Theta_u - \tilde{\Theta}_u\right) + 0.2785\delta_{\vartheta_r}\tilde{\Theta}_r + \vartheta_r\tilde{\Theta}_r\left(\Theta_r - \tilde{\Theta}_r\right) \\ & + 0.2785\delta_{\phi_u}\tilde{\xi}_{d_u} + \phi_u\tilde{\xi}_{d_u}\left(\xi_{d_u} - \tilde{\xi}_{d_u}\right) + 0.2785\delta_{\phi_r}\tilde{\xi}_{d_r} + \phi_r\tilde{\xi}_{d_r}\left(\xi_{d_r} - \tilde{\xi}_{d_r}\right) \\ & - \frac{\left(e_u^f\right)^2}{\kappa_u} + e_u^f P_u - \frac{\left(e_r^f\right)^2}{\kappa_r} + e_r^f P_r \end{aligned} \quad (25)$$

According to Young's inequality, Eq. (25) can become

$$\begin{aligned} \dot{H} \leq {} & -\eta_{11}z_e^2 - \eta_{12}|z_e|^{\upsilon+1} - \eta_{21}\varphi_e^2 - \eta_{22}|\varphi_e|^{\upsilon+1} - \eta_{31}u_e^2 - \eta_{32}|u_e|^{\upsilon+1} - \eta_{41}r_e^2 - \eta_{42}|r_e|^{\upsilon+1} \\ & - \frac{\vartheta_u}{2}\tilde{\Theta}_u^2 + \frac{\vartheta_u\left(\Theta_u + 0.2785\delta_{\vartheta_u}\vartheta_u^{-1}\right)^2}{2} - \frac{\vartheta_r}{2}\tilde{\Theta}_r^2 + \frac{\vartheta_r\left(\Theta_r + 0.2785\delta_{\vartheta_r}\vartheta_u^{-1}\right)^2}{2} \\ & - \frac{\phi_u}{2}\tilde{\xi}_{d_u}^2 + \frac{\phi_u\left(\xi_{d_u} + 0.2785\delta_{\phi_u}\phi_u^{-1}\right)^2}{2} - \frac{\phi_r}{2}\tilde{\xi}_{d_r}^2 + \frac{\phi_r\left(\xi_{d_r} + 0.2785\delta_{\phi_r}\phi_r^{-1}\right)^2}{2} \\ & - \omega_u\left(e_u^f\right)^2 - \omega_r\left(e_r^f\right)^2 \end{aligned} \quad (26)$$

where $\omega_u = \frac{1}{\kappa_u} - \frac{1}{2}P_u^2$ and $\omega_r = \frac{1}{\kappa_r} - \frac{1}{2}P_r^2$.

By further simplifying Eq. (26), we can obtain

$$\begin{aligned}\dot{H} \le & -\eta_{11} z_e^{\,2} - \eta_{12} \left| z_e \right|^{\upsilon+1} - \eta_{21} \varphi_e^{\,2} - \eta_{22} \left| \varphi_e \right|^{\upsilon+1} - \eta_{31} u_e^{\,2} - \eta_{32} \left| u_e \right|^{\upsilon+1} - \eta_{41} r_e^{\,2} - \eta_{42} \left| r_e \right|^{\upsilon+1} \\ & - \frac{\vartheta_u}{4} \tilde{\Theta}_u^{\,2} - \frac{\vartheta_r}{4} \tilde{\Theta}_r^{\,2} - \frac{\vartheta_u}{2(\upsilon+1)} \left| \tilde{\Theta}_u \right|^{\upsilon+1} - \frac{\vartheta_r}{2(\upsilon+1)} \left| \tilde{\Theta}_r \right|^{\upsilon+1} + \frac{(1-\upsilon)(\vartheta_u + \vartheta_r)}{4(\upsilon+1)} \\ & - \frac{\phi_u}{4} \tilde{\xi}_{d_u}^{\,2} - \frac{\phi_r}{4} \tilde{\xi}_{d_r}^{\,2} - \frac{\phi_u}{2(\upsilon+1)} \left| \tilde{\xi}_{d_u} \right|^{\upsilon+1} - \frac{\phi_r}{2(\upsilon+1)} \left| \tilde{\xi}_{d_r} \right|^{\upsilon+1} + \frac{(1-\upsilon)(\phi_u + \phi_r)}{4(\upsilon+1)} \\ & - \frac{\omega_u}{2} \left(e_u^{\,f} \right)^2 - \frac{\omega_r}{2} \left(e_r^{\,f} \right)^2 - \frac{\omega_u}{\upsilon+1} \left| e_u^{\,f} \right|^{\upsilon+1} - \frac{\omega_r}{\upsilon+1} \left| e_r^{\,f} \right|^{\upsilon+1} + \frac{(1-\nu)(\omega_u + \omega_r)}{2(\nu+1)} \\ & + \frac{\vartheta_u \left(\Theta_u + 0.2785 \delta_{\vartheta_u} \vartheta_u^{-1} \right)^2}{2} + \frac{\vartheta_r \left(\Theta_r + 0.2785 \delta_{\vartheta_r} \vartheta_u^{-1} \right)^2}{2} \\ & + \frac{\phi_u \left(\xi_{d_u} + 0.2785 \delta_{\phi_u} \phi_u^{-1} \right)^2}{2} + \frac{\phi_r \left(\xi_{d_r} + 0.2785 \delta_{\phi_r} \phi_r^{-1} \right)^2}{2} \\ & = \upsilon_1 V - \upsilon_2 V^{\frac{\upsilon+1}{2}} + \Omega \end{aligned} \tag{27}$$

where

$$\upsilon_1 = \min \left\{ 2\eta_{11}, 2\eta_{21}, 2\eta_{31}, 2\eta_{41}, \frac{\vartheta_u}{2}, \frac{\vartheta_r}{2}, \frac{\phi_u}{2}, \frac{\phi_r}{2}, \omega_u, \omega_r \right\},$$

$$\upsilon_2 = 2^{\frac{\upsilon+1}{2}} \left\{ \eta_{12}, \eta_{22}, \eta_{32}, \eta_{42}, \frac{\vartheta_u}{2(\upsilon+1)}, \frac{\vartheta_r}{2(\upsilon+1)}, \frac{\phi_u}{2(\upsilon+1)}, \frac{\phi_r}{2(\upsilon+1)}, \frac{\omega_u}{\upsilon+1}, \frac{\omega_r}{\upsilon+1} \right\},$$

$$\begin{aligned} \Omega = & \frac{(1-\upsilon)(\vartheta_u + \vartheta_r)}{4(\upsilon+1)} + \frac{(1-\upsilon)(\phi_u + \phi_r)}{4(\upsilon+1)} + \frac{(1-\nu)(\omega_u + \omega_r)}{2(\nu+1)} + \frac{\vartheta_u \left(\Theta_u + 0.2785 \delta_{\vartheta_u} \vartheta_u^{-1} \right)^2}{2} \\ & + \frac{\vartheta_r \left(\Theta_r + 0.2785 \delta_{\vartheta_r} \vartheta_u^{-1} \right)^2}{2} + \frac{\phi_u \left(\xi_{d_u} + 0.2785 \delta_{\phi_u} \phi_u^{-1} \right)^2}{2} + \frac{\phi_r \left(\xi_{d_r} + 0.2785 \delta_{\phi_r} \phi_r^{-1} \right)^2}{2} \end{aligned}$$

According to Eq. (27), we can obtain

$$\dot{H} \le -\iota \upsilon_1 H - (1-\iota) \upsilon_1 H - \upsilon_2 H^{\frac{\vartheta}{2}} + \Omega \tag{28}$$

where $\iota = \min \{ \iota_1, \iota_2 \}$ ($0 < \iota < 1$).

If $H > \dfrac{\Omega}{\iota \upsilon_1}$, then

$$\dot{H} \le -(1-\iota) \upsilon_1 H - \upsilon_2 H^{\vartheta} \tag{29}$$

According to Lemma 1, the system will stabilize to area $\Omega_L = \left\{ L : L \le \dfrac{\Omega}{\dot{\chi} \upsilon_1} \right\}$ within finite time, and the stabilization time is as follows:

$$T \le \frac{4}{(1-\iota)\upsilon_1} \ln \left[\frac{(1-\iota)\upsilon_1 H^{\frac{1-\upsilon}{2}}(0) + \upsilon_2}{\upsilon_2} \right] \tag{30}$$

From Eq. (20), we can obtain

$$\begin{cases} \dfrac{d}{dt} \left| e_u \right| = \dfrac{d}{dt} \left(e_u * e_u \right) = \operatorname{sgn}(e_u) \dot{e}_u \le \left| \dot{L}_u(t) \right| \\ \dfrac{d}{dt} \left| e_r \right| = \dfrac{d}{dt} \left(e_r * e_r \right) = \operatorname{sgn}(e_r) \dot{e}_r \le \left| \dot{L}_r(t) \right| \end{cases} \tag{31}$$

Since the $\dot{L}_i$ ($i = u, r$) are smoothly differentiable functions, $\dot{L}_i$ is a continuous function. Since all its variables are globally bounded, $\lambda_i > 0$ makes $\left| \dot{L}_i \right| \le \lambda_i$. When $t = t_k$, $e_i(t_k) = 0$ and $\lim\limits_{t \to t_k} e_i(t) = \eta_i$. Therefore, there is a time interval $t_k^{\,*}$ that satisfies $t^* \ge \dfrac{\eta_i}{\lambda_i}$. In summary, Zeno's behaviour will not occur.

SIMULATION

In the simulation stage, the Cybership 2 ship model of the Norwegian University of Science and Technology was selected as the controlled object, and its parameters are detailed in [30]. To verify the effectiveness of the designed finite-time trajectory-tracking control scheme, the time-varying disturbance given in Eq. (32) is selected to simulate the external uncertain interference in actual navigation:

$$\begin{cases} d_u = \left[1 + 0.5 \sin(0.2t) + 0.2 \cos(0.5t) \right] \\ d_v = \left[1 + 0.3 \sin(0.2t) + 0.3 \cos(0.2t) \right] \\ d_r = \left[1 + 0.4 \sin(0.3t) + 0.2 \cos(0.3t) \right] \end{cases} \tag{32}$$

The system's FDIA signals are set as follows:

$$\begin{cases} \xi_u = 0.2 + 0.2 \sin(0.2t) \\ \xi_r = 0.15 + 0.3 \cos(0.1t) \end{cases} \tag{33}$$

The control parameters are detailed in Table 1.

Tab. 1. Controller parameters

$\eta_{11} = 0.3$	$\eta_{12} = 0.1$	$\eta_{21} = 0.3$	$\eta_{22} = 0.1$	$\nu = 0.5$	$\kappa_u = 0.01$	$\kappa_r = 0.1$
$\kappa_r = 0.01$	$\eta_{31} = 0.3$	$_{32}$ 0.5	$\mu_u = 1$	$\vartheta_u = 0.01$	$\delta_{\vartheta_u} = 0.03$	$\varepsilon_u = 1$
$\phi_u = 0.02$	$\delta_{\phi_u} = 0.02$	$\eta_{41} = 0.5$	$\eta_{42} = 0.3$	$\mu_r = 1.5$	$\vartheta_r = 0.01$	$\delta_{\vartheta_r} = 0.02$
$\varepsilon_r = 1$	$\phi_r = 0.01$	$\delta_{\phi_r} = 0.02$	$\eta_u = 0.02$	$\eta_r = 0.3$		

To carry out the quantitative and qualitative analysis of the control scheme designed in this article, we introduce the integrated absolute error (IAE) and mean integrated absolute control (MIAC) in Eq. (35) to evaluate the steady-state performance and energy consumption performance. The evaluation results are shown in Tables 2 and 3:

$$\begin{cases} \text{IAE} = \int_0^{t_f} |\upsilon_e| dt, \upsilon = x, y \\ \text{MIAC} = \dfrac{1}{t_f} \int_0^{t_f} |\tau_i(t)| dt, i = u.r \end{cases} \tag{35}$$

Simulation experiment 1

In simulation experiment 1, we set the simulation time to 200 s and the step size to 0.01.

The circular reference trajectory is as follows:

$$\begin{cases} x_d = 50 \sin(0.01\pi t) \\ y_d = 50 - 50 \cos(0.01\pi t) \end{cases} \tag{34}$$

Tab. 2. Performance index comparison of the control schemes for simulation 1

		ETC scheme	Continuous scheme	The scheme in [25]
IAE	x_e	10.23	10.15	11.37
	y_e	9.52	9.26	10.29
MIAC	τ_u	1.36	1.41	1.39
	τ_r	1.12	1.33	1.28

The simulation results of this study are shown in Figures 2–10. Figures 2 and 3 show the effects of three different control schemes for completing tracking tasks. They show that each control scheme successfully completed the established tracking task within a limited time, confirming the effectiveness of the control scheme.

Figure 4 shows the trend of the system velocity with time under these three control schemes. The results show that as time progresses, the system velocity under all control schemes gradually tends toward a bounded stable state.

The time course of the systematic error is shown in Figures 5 and 6. These curves clearly show the performance comparison under different control schemes. The continuous control scheme designed in this article shows the best effect in terms of the control performance, followed by the ETC scheme designed in this article. In contrast, the control effects of these two schemes are better than the control scheme proposed in [25].

Figure 7 shows the duration curve of the system control input. It can be observed from the figure that as time goes by, the control inputs of the three control schemes stabilize within a relatively small interval. This shows the stability and reliability of the control scheme. Figures 7 and 10 further demonstrate the advantages of the ETC control scheme in terms of the controller update frequency compared to the other two continuous control schemes. In the ETC control scheme, the controller is updated only 2611 times and 986 times. For both continuous control schemes, the number of controller updates is 20,000 times. This means that the ETC scheme can achieve effective control with a lower update frequency, thereby more effectively solving the communication resource limitation problem. In addition, according to the comparison of the performance indicators in Table 2, it can be concluded that the IAE value is the smallest in the continuous control scheme designed in this paper, followed by the ETC scheme and finally the scheme in [25]. The MIAC value is the smallest for the ETC scheme, followed by the scheme in [25] and finally the ETC scheme. This means that the tracking accuracy of the two control schemes is significantly improved compared to the scheme in [25]. However, the energy consumption of the continuous control scheme designed in this article is slightly higher. The ETC control scheme has significant improvements in terms of both the tracking accuracy and energy consumption.

Figures 8 and 9 show the approximation effect of the approximator on FDIAs, external disturbances, and dynamic uncertainties in the system. These plots show that the upper bounds of all uncertainties are effectively estimated, thereby enhancing the robustness of the control scheme.

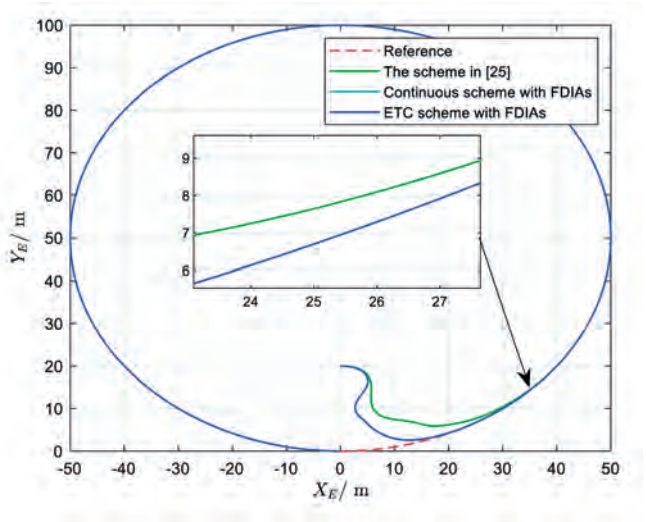

Fig. 2 Actual and reference trajectories in the (x, y) plane

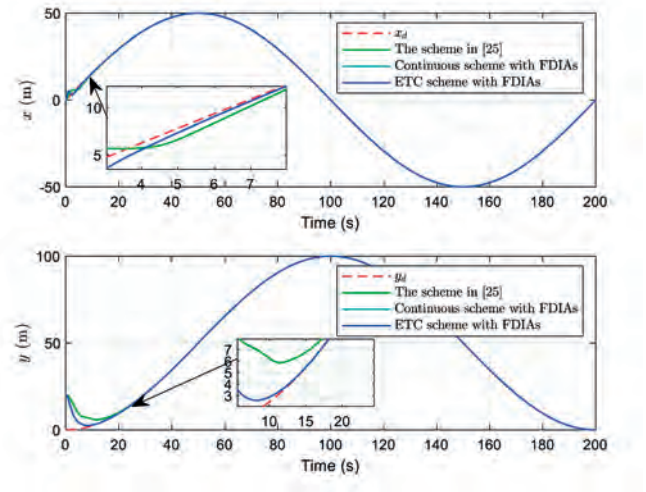

Fig. 3. Actual and reference positions

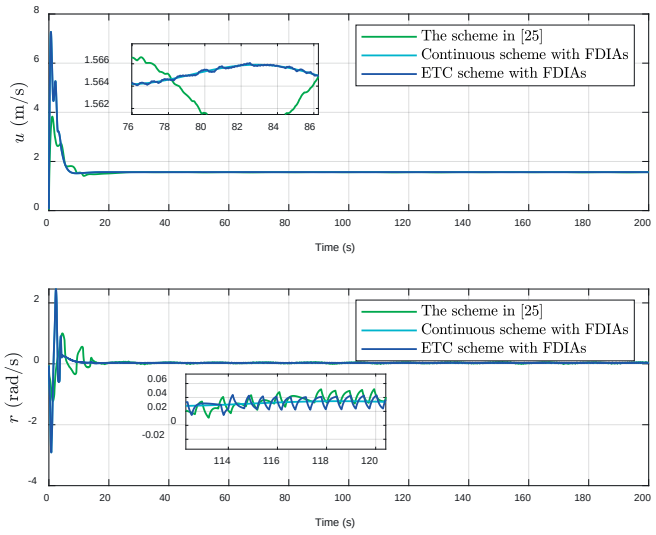

Fig. 4. Vessel velocity duration curve

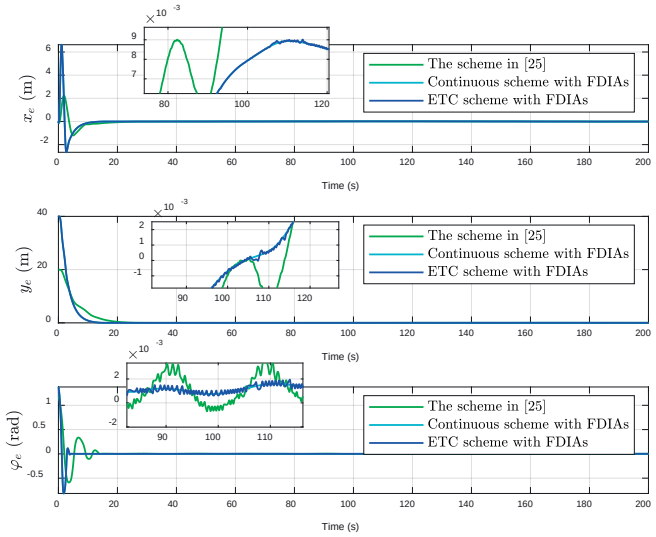

Fig. 5. Time evolution of the attitude errors

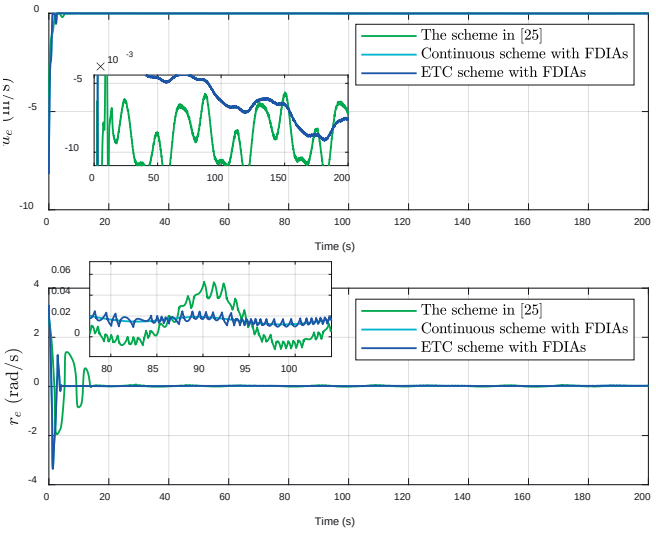

Fig. 6. Time evolution of the velocity errors

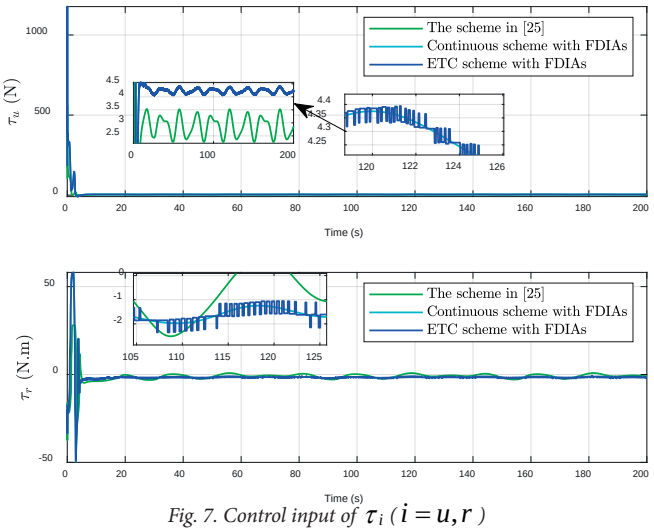

Fig. 7. Control input of τ_i ($i = u, r$)

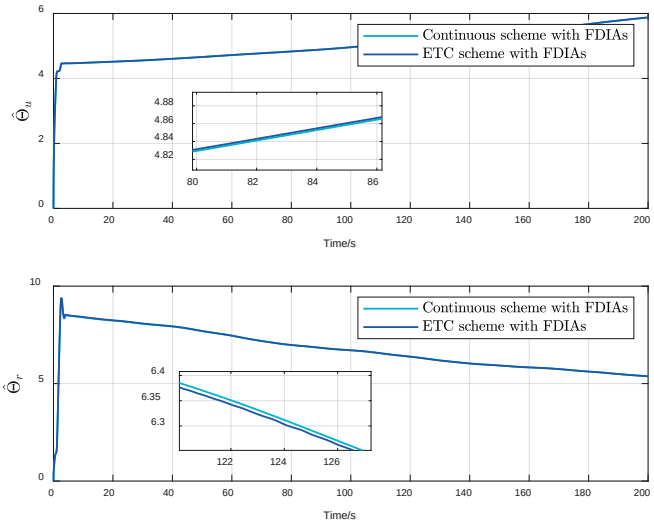

Fig. 8. Estimated values of Θ_u and Θ_r

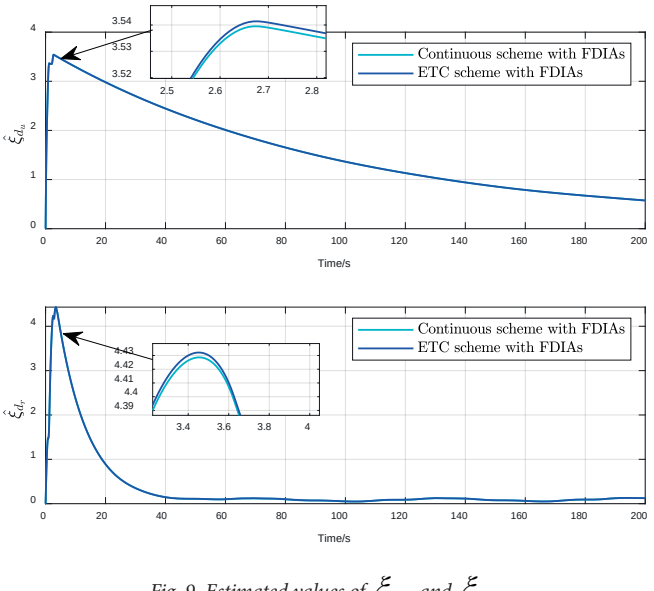

Fig. 9. Estimated values of ξ_{d_u} and ξ_{d_u}

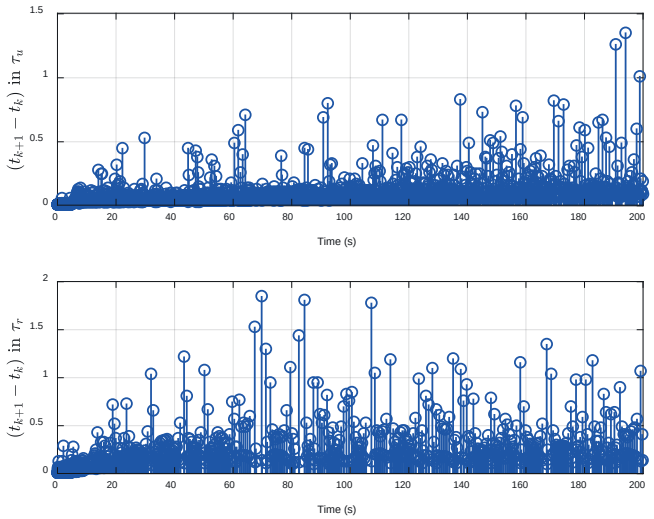

Fig. 10. Time evolution of the inter-event time

Simulation experiment 2

In simulation experiment 2, we set the simulation time to 100 s and the step size to 0.01.

The reference trajectory is as follows:

$$\begin{cases} x_d = 10\sin(0.02\pi t) \\ y_d = 6\sin(0.04\pi t) \end{cases} \tag{34}$$

Tab. 3 Performance index comparison of the control schemes for simulation 2

		ETC scheme	Continuous scheme	The scheme in [25]
IAE	x_e	11.15	11.02	12.21
	y_e	10.35	10.02	11.31
MIAC	τ_u	1.45	1.52	1.49
	τ_r	1.31	1.38	1.35

The simulation results are shown in Figures 11–20. Figures 11 and 12 show the tracking effects of the three control schemes on the reference trajectory. They all completed the tracking task excellently. However, the control scheme designed in this article can track the reference trajectory more quickly. Figure 13 shows the velocity changes of the three control schemes. They all tend to be bounded over time. Figures 14 and 15 show the tracking error of the system. The tracking accuracy of the control scheme designed in this paper is significantly higher than that of the control scheme in [25]. By analyzing the performance indicators in Table 2, we can conclude that the continuous control method designed in this article has the highest tracking accuracy, followed by the ETC scheme designed in this article. The method in [25] is slightly inferior in terms of tracking progress. From the perspective of energy consumption, the ETC method is the most energy-saving, followed by the control scheme in [25] and finally the continuous control scheme designed in this paper. Although the continuous control scheme has the highest control accuracy, it is accompanied by high energy consumption. The ETC method takes into account the advantages of lower energy consumption and higher tracking accuracy.

According to Figures 16 and 19, it can be concluded that the update frequency of the ETC scheme controller has been greatly reduced. In the continuous control scheme and the control scheme in [25], the number of controller updates is 10,000, while in the ETC scheme, it is only 603 and 607. Figure 17 shows the adaptive curve of the system dynamic uncertainty. Figure 18 shows the approximation effect of the system on the composite uncertainty dynamics composed of external disturbances and FDIAs. They are all effectively estimated.

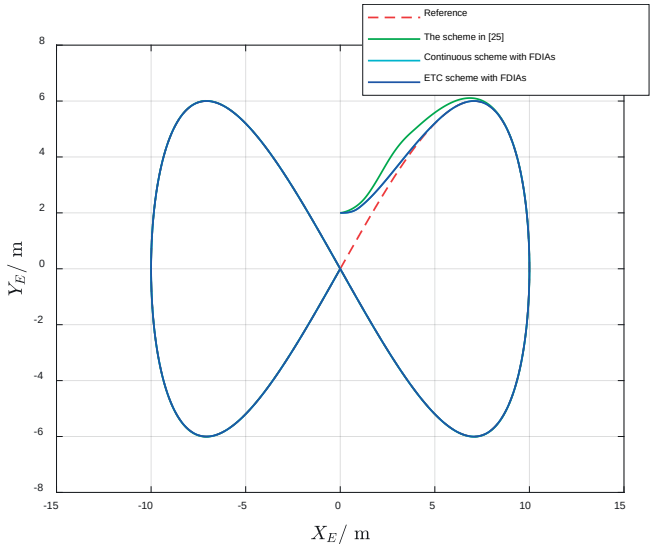

Fig. 11. Actual and reference trajectories in the (x, y) plane

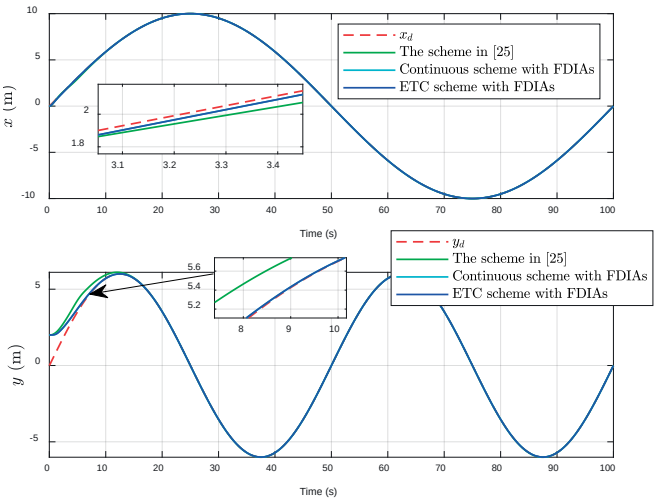

Fig. 12. Actual and reference positions

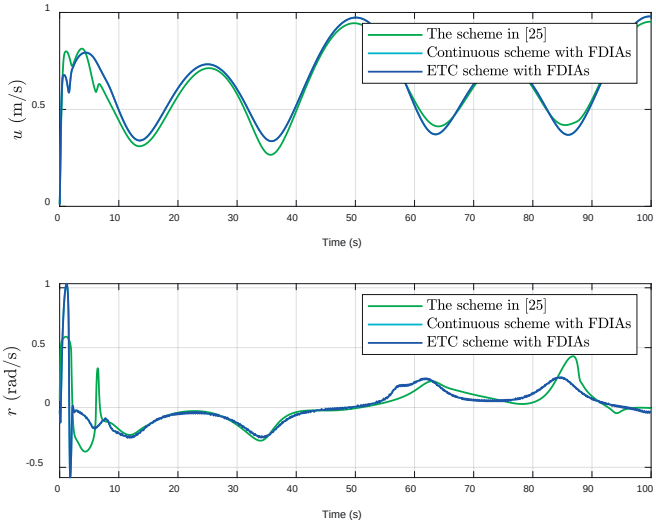

Fig. 13. Vessel velocity duration curve

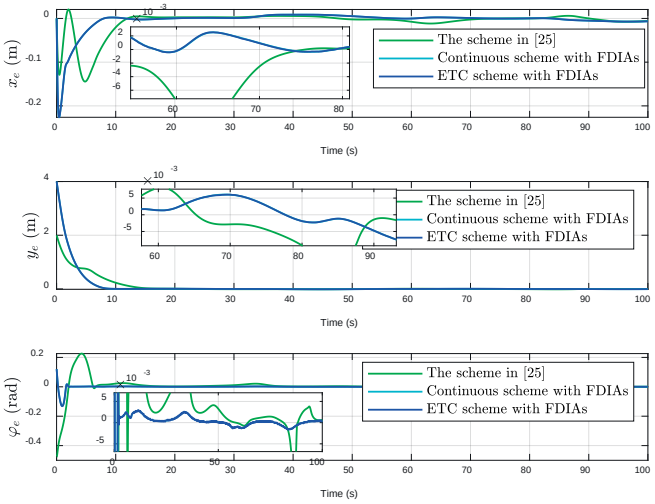

Fig. 14. Time evolution of the attitude errors

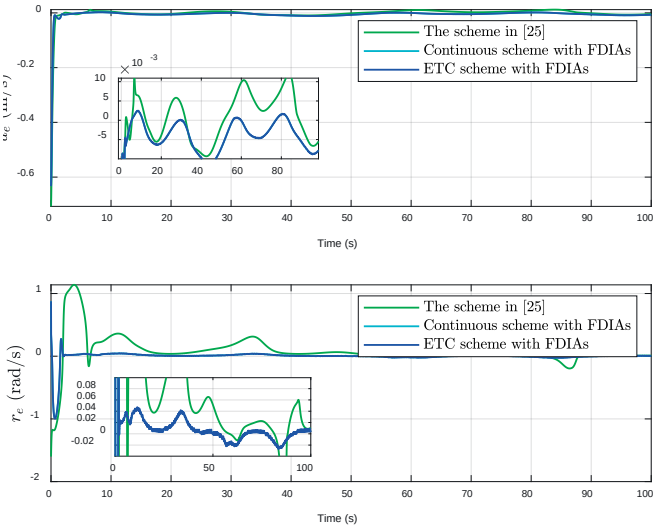

Fig. 15. Time evolution of the velocity errors

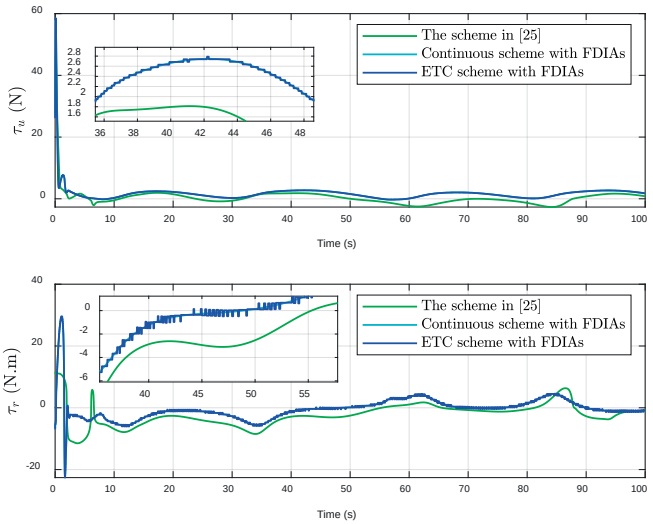

Fig. 16. Control input of τ_i ($i = u, r$)

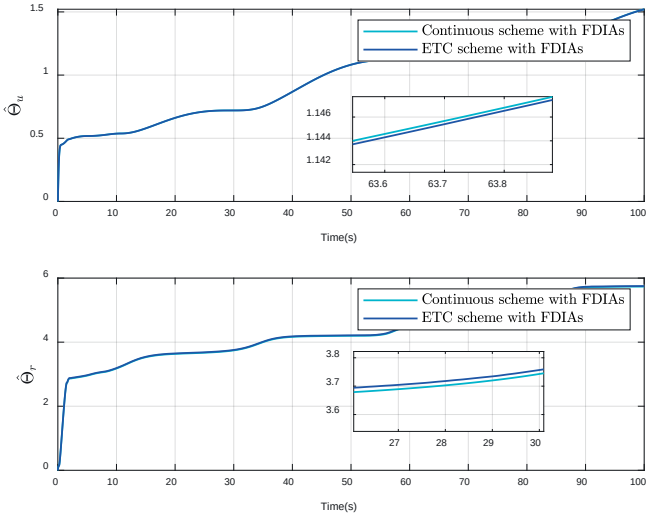

Fig. 17. Estimated values of Θ_u and Θ_r

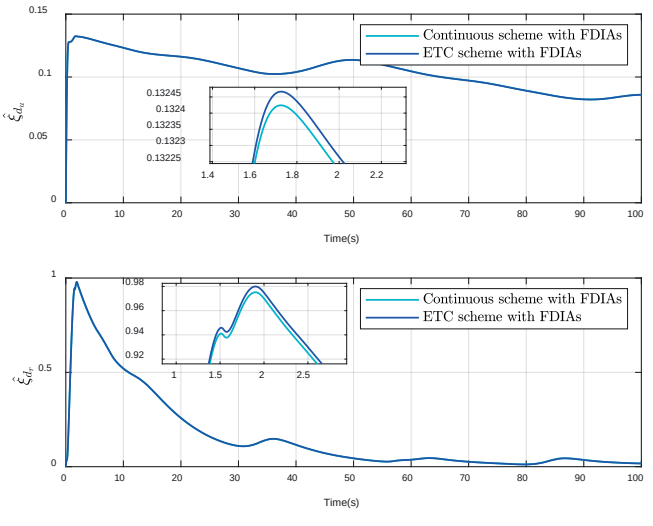

Fig. 18. Estimated values of ξ_{d_u} and ξ_{d_u}

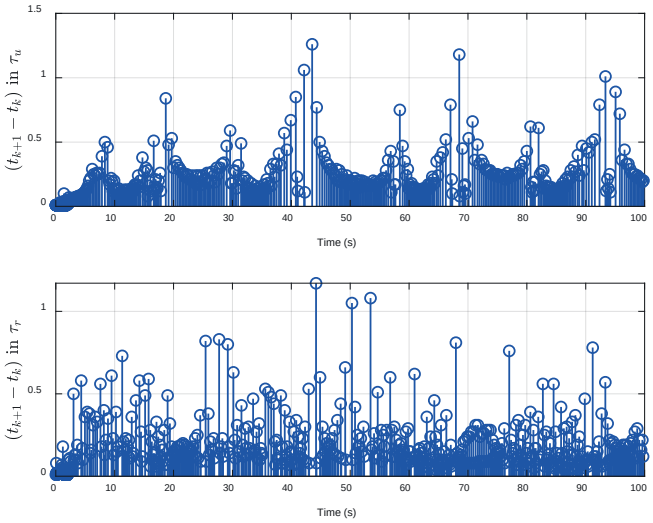

Fig. 19. Time evolution of the inter-event time

CONCLUSION

This paper studies the USV trajectory-tracking control problem constrained by FDIAs and internal and external uncertainties. Uncertain dynamics, including FDIAs, are compensated through the design of online approximators. At the same time, to optimize the tracking performance of the system, we also introduced FTC and ETC technologies. They improve the steady-state performance of the system and save the communication resources of the system. They ensure that the system can still complete control tasks with high precision under the constraints of limited communication resources. The main contributions of this article are as follows:

(1) This paper solves the trajectory-tracking control problem of USVs under the influence of FDIAs for the first time. Compared with [1], [2], this method can effectively cope with and resist the adverse effects of FDIAs, ensuring that USVs can still accurately track the predetermined trajectory when they are attacked.

(2) This paper incorporates FTC technology into the design process of the control scheme. Compared with [8], [13], this scheme ensures that USVs can quickly adjust when they face emergencies, thereby meeting the need for rapid response.

(3) This paper organically combines FTC technology and ETC technology. Compared with [15], [16], this scheme provides the system with rapid response capabilities for emergencies and external disturbances. The ETC mechanism ensures that control is only performed at critical moments while also greatly reducing the computing and communication requirements, making the control system more energy-saving and efficient.

Overall, our research provides an efficient and stable trajectory-tracking control scheme for USVs disturbed by FDIAs and internal and external uncertainties, providing new ideas for research and practical applications in this field.

However, the types of attacks covered in this study are limited to FDIAs targeting actuators. In the future, we hope to expand the attack objects to the output of the system and introduce more attack types, such as deception attacks and denial of service attacks.

FUNDING

This work was supported by the Education and Research Project for Middle and Young Teachers in Fujian Province (No. JAT210241).

REFERENCES

1. S. L. Yu, J. S. Lu, G. B. Zhu and S. J. Yang, 'Event-triggered finite-time tracking control of underactuated MSVs based on neural network disturbance observer', *Ocean Engineering*, 2022, doi: 10.1016/j.oceaneng.2022.111169.

2. X. F. Meng, G. C. Zhang and Q. Zhang, 'Event-triggered trajectory tracking control of underactuated surface vessels with performance-improving mechanisms under input saturation and actuator faults', *Transactions of the Institute of Measurement and Control*, 2023, doi: 10.1177/01423312231187008.

3. Z. H. Yu and W. L. Chin, 'Blind false data injection attack using PCA approximation method in smart grid,' *IEEE Transactions on Smart Grid,* vol. 6, no. 3, pp. 1219–1226, 2015, doi: 10.1109/TSG.2014.2382714.

4. Q. T. Yin, Y. X. Bian, J. Du, W. Zhao and S. B. Yang, 'Dual backstepping variable structure switching control of bounded uncertain nonlinear system', *International Journal of Systems Science*, vol. 53, no. 11, pp. 2341–2357, 2022, doi: 10.1080/00207721.2022.2051094.

5. R. Rout, R. X. Cui and W. S. Yan, 'Sideslip-compensated guidance-based adaptive neural control of marine surface vessels', *IEEE Transactions on Cybernetics,* vol. 52, no. 5, pp. 2860–2871, 2022, doi: 10.1109/TCYB.2020.3023162.

6. D. Menges and A. Rasheed, 'An environmental disturbance observer framework for autonomous surface vessels', *Ocean Engineering,* vol. 285, 2023, doi: 10.1016/j.oceaneng.2023.115412.

7. C. Zhang and S. H. Yu, 'Disturbance observer-based prescribed performance super-twisting sliding mode control for autonomous surface vessels', *ISA Transactions*, vol. 135, pp. 13–22, 2023, doi: 10.1016/j.isatra.2022.09.025.

8. X. W. Wang, J. Liu, H. J. Peng, X. W. Qie, X. D. Zhao and C. Lu 'A simultaneous planning and control method integrating APF and MPC to solve autonomous navigation for USVs in unknown environments', *Journal of Intelligent & Robotic Systems,* vol. 105, no. 2, 2022, doi: 10.1007/s10846-022-01663-8.

9. X. Han and X. K. Zhang, 'Tracking control of ship at sea based on MPC with virtual ship bunch under Frenet frame', *Ocean Engineering*, 2022, doi: 10.1016/j.oceaneng.2022.110737.

10. W. R. Wang, J. H. Yan, H. Wang, H. L. Ge, Z. Y. Zhu and G. J. Yang, 'Adaptive MPC trajectory tracking for AUV based on Laguerre function', *Ocean Engineering*, 2022, doi: 10.1016/j.oceaneng.2022.111870.

11. E. Tatlicioglu, B. M. Yilmaz, A. Savran and M. Alci, 'Adaptive fuzzy logic with self-adjusting membership functions based tracking control of surface vessels', *Ocean Engineering,* 2022, doi: 10.1016/j.oceaneng.2022.111129.

12. X. F. Meng, G. C. Zhang and Q Zhang, 'Robust adaptive neural network integrated fault-tolerant control for underactuated surface vessels with finite-time convergence and event-triggered inputs', *Mathematical Biosciences and Engineering,* vol. 20, no. 2, pp. 2131–2156, 2023, doi: 10.3934/mbe.2023099.

13. Y. Fang, E, Zergeroglu, M. S. de. Queiroz and D. M. Dawson, 'Global output feedback control of dynamically positioned surface vessels: an adaptive control approach. Mechatronics', *Mechatronics,* vol. 14, no. 4, pp. 341–356, 2004, doi: 10.1016/S0957-4158(03)00064-3.

14. G. B. Zhu, Y. Ma, Z. X. Li, R. Malekian and Sotelo M, 'Adaptive neural output feedback control for MSVs with predefined performance', *IEEE Transactions on Vehicular Technology,* vol. 70, no. 4 pp. 2994–3006, 2021, doi: 10.1109/TVT.2021.3063687.

15. G. B. Zhu, Y. Ma and S. L. Hu, 'Single-parameter-learning-based finite-time tracking control of underactuated MSVs under input saturation', *Control Engineering Practice,* 2020, doi: 10.1016/j.conengprac.2020.104652.

16. Y. L. Yu, C. Guo and T. S. Li, 'Finite-time LOS path following of unmanned surface vessels with time-varying sideslip angles and input saturation', *IEEE-ASME Transactions on Mechatronics,* vol. 27, no. 1, pp. 463–474, 2022, doi: 10.1109/TMECH.2021.3066211.

17. M, Van, V. T. Do, M. O. Khyam and Do XP, 'Tracking control of uncertain surface vessels with global finite-time convergence', *Ocean Engineering,* 2021, doi: 10.1016/j.oceaneng.2021.109974.

18. X. F. Meng, G. C. Zhang and B. Han, 'Fault-tolerant control of underactuated MSVs based on neural finite-time disturbance observer: An Event-triggered Mechanism', *Journal of the Franklin Institute,* 2024, doi: 10.1016/j.jfranklin.2024.01.004.

19. Y. J. Deng, X. K. Zhang, N. Im, G. Q. Zhang and Q. Zhang, 'Model-based event-triggered tracking control of underactuated surface vessels with minimum learning parameters', *IEEE Transactions on Neural Networks and Learning Systems*', vol. 31, no. 10, pp. 4001–4014, 2020, doi: 10.1109/TNNLS.2019.2951709.

20. G. B. Zhu, Y. Ma and S. L. Hu, 'Event-triggered adaptive PID fault-tolerant control of underactuated ASVs under saturation constraint', *IEEE Transactions on Systems Man Cybernetics-Systems*, vol. 53, no. 8, pp. 4922–4933, 2023, doi: 10.1109/TSMC.2023.3256538.

21. N. Feng, D. F. Wu, H. L. Yu, A. S. Yamashita and Y. Q. Huang, 'Predictive compensator based event-triggered model predictive control with nonlinear disturbance observer for unmanned surface vehicle under cyber-attacks', Ocean Engineering, vol. 259, 2022, doi: 10.1016/j.oceaneng.2022.111868.

22. Y. X. Zheng, L. Zhang, B. Huang and Y. M. Su, 'Distributed secure formation control for autonomous surface vessels by performance adjustable event-triggered mechanism', International Journal of Robust and Nonlinear Control, vol. 33, no. 14, pp. 8490–8507, 2023, doi: 10.1002/rnc.6832.

23. G. Q. Zhang, X. J. Dong, Q. H. Shan and W. D. Zhang, 'Event-triggered robust adaptive control for unmanned surface vehicle in presence of deception attacks', Proceedings of the Institution of Mechanical Engineers Part I-Journal of Systems and Control Engineering, vol. 237, no. 7, pp. 1266–1280, 2023, doi: 10.1177/09596518231153437.

24. T. I. Fossen, Handbook of marine craft hydrodynamics and motion control, 2011.

25. Y. Ma, G. B. Zhu and Z. X. Li, 'Error-driven-based nonlinear feedback recursive design for adaptive NN trajectory tracking control of surface ships with input saturation', IEEE Intelligent Transportation Systems Magazine, 2019, vol. 11, no. 2, pp. 17–28, doi: 10.1109/MITS.2019.2903517.

26. K. X. Huang, C. J. Zhou, Y. Q. Qin and W. X. Tu, 'A game-theoretic approach to cross-layer security decision-making in industrial cyber-physical systems', IEEE Transactions on Industrial Electronics, vol. 67, no. 2, pp. 2371–2379, 2020, doi: 10.1109/TIE.2019.2907451.

27. S. H. Yu, X. H. Yu, B. Shirinzadeh and Z. H. Man, 'Continuous finite time control for robotic manipulators with terminal sliding mode', *Automatica,* vol. 41, no. 11, pp. 1957–1964, 2005, doi: 10.1016/j.automatica.2005.07.001.

28. M. M. Polycarpou, 'Stable adaptive neural control scheme for nonlinear systems', *IEEE Transactions on Automatic Control,* vol. 41, no. 3, pp. 447–451, 1996, doi: 10.1109/9.486648.

29. X. F. Meng, G. C. Zhang, Q. Zhang and B. Han, 'Event-triggered adaptive command-filtered trajectory tracking control for underactuated surface vessels based on multivariate finite-time disturbance observer under actuator faults and input saturation', *Transactions of the Institute of Measurement and Control*, 2024, doi: 10.1177/01423312231195657.

30. R. Skjetne, T. I. Fossen and P. V. Kokotovic, 'Adaptive maneuvering, with experiments, for a model ship in a marine control laboratory', *Automatica*, vol. 41, no. 2, pp. 289–298, 2005, doi: 10.1016/j.automatica.2004.10.006.